

## D-T gamma-to-neutron branching ratio determined from inertial confinement fusion plasmas

Y. Kim, J. M. Mack, H. W. Herrmann, C. S. Young, G. M. Hale et al.

Citation: *Phys. Plasmas* **19**, 056313 (2012); doi: 10.1063/1.4718291

View online: <http://dx.doi.org/10.1063/1.4718291>

View Table of Contents: <http://pop.aip.org/resource/1/PHPAEN/v19/i5>

Published by the [American Institute of Physics](http://www.aip.org).

---

### Related Articles

Hot-spot mix in ignition-scale implosions on the NIF

*Phys. Plasmas* **19**, 056307 (2012)

Experimental and theoretical evaluation of surface coated exploding wires

*Phys. Plasmas* **19**, 032702 (2012)

Spatiotemporal temperature and density characterization of high-power atmospheric flashover discharges over inert poly(methyl methacrylate) and energetic pentaerythritol tetranitrate dielectric surfaces

*J. Appl. Phys.* **111**, 053303 (2012)

High-current discharge channel contraction in high density gas

*Phys. Plasmas* **18**, 122702 (2011)

Generating extra long arcs using exploding wires

*J. Appl. Phys.* **110**, 093303 (2011)

---

### Additional information on Phys. Plasmas

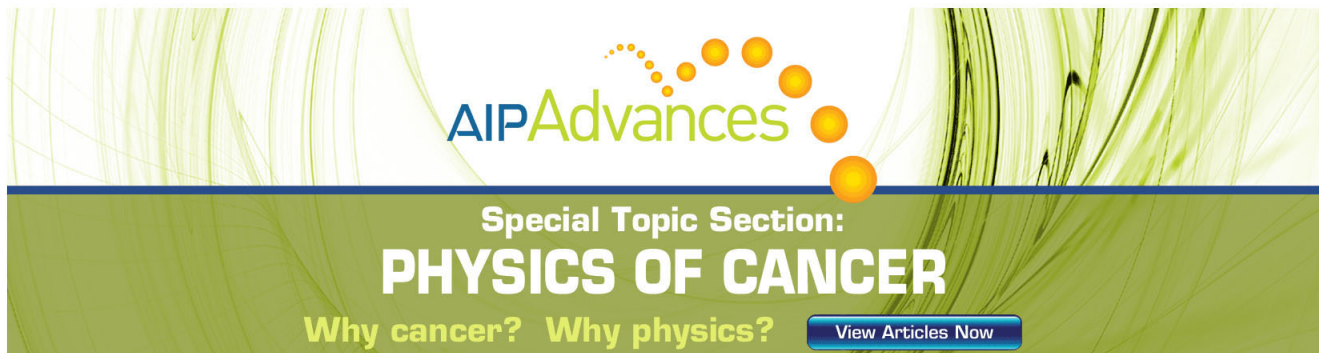
Journal Homepage: <http://pop.aip.org/>

Journal Information: [http://pop.aip.org/about/about\\_the\\_journal](http://pop.aip.org/about/about_the_journal)

Top downloads: [http://pop.aip.org/features/most\\_downloaded](http://pop.aip.org/features/most_downloaded)

Information for Authors: <http://pop.aip.org/authors>

## ADVERTISEMENT



**AIP Advances**

Special Topic Section:  
**PHYSICS OF CANCER**

Why cancer? Why physics? [View Articles Now](#)

# D-T gamma-to-neutron branching ratio determined from inertial confinement fusion plasmas<sup>a)</sup>

Y. Kim,<sup>1,b)</sup> J. M. Mack,<sup>1</sup> H. W. Herrmann,<sup>1</sup> C. S. Young,<sup>1</sup> G. M. Hale,<sup>1</sup> S. Caldwell,<sup>1</sup> N. M. Hoffman,<sup>1</sup> S. C. Evans,<sup>1</sup> T. J. Sedillo,<sup>1</sup> A. McEvoy,<sup>1</sup> J. Langenbrunner,<sup>1</sup> H. H. Hsu,<sup>1</sup> M. A. Huff,<sup>1</sup> S. Batha,<sup>1</sup> C. J. Horsfield,<sup>2</sup> M. S. Rubery,<sup>2</sup> W. J. Garbett,<sup>2</sup> W. Stoeffl,<sup>3</sup> E. Grafil,<sup>3</sup> L. Bernstein,<sup>3</sup> J. A. Church,<sup>3</sup> D. B. Sayre,<sup>3</sup> M. J. Rosenberg,<sup>4</sup> C. Waugh,<sup>4</sup> H. G. Rinderknecht,<sup>4</sup> M. Gatu Johnson,<sup>4</sup> A. B. Zylstra,<sup>4</sup> J. A. Frenje,<sup>4</sup> D. T. Casey,<sup>4</sup> R. D. Petrasso,<sup>4</sup> E. Kirk Miller,<sup>5</sup> V. Yu Glebov,<sup>6</sup> C. Stoeckl,<sup>6</sup> and T. C. Sangster<sup>6</sup>

<sup>1</sup>Los Alamos National Laboratory, Los Alamos, New Mexico 87545, USA

<sup>2</sup>Atomic Weapons Establishment, Aldermaston, Reading, Berkshire RG7 4PR, United Kingdom

<sup>3</sup>Lawrence Livermore National Laboratory, Livermore, California 94550, USA

<sup>4</sup>Plasma Science and Fusion Center, Massachusetts Institute of Technology, Cambridge, Massachusetts 02139, USA

<sup>5</sup>National Security Technologies, LLC, Special Technologies Laboratory, Santa Barbara, California 93111, USA

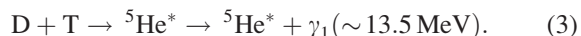
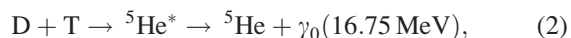
<sup>6</sup>Laboratory for Laser Energetics, University of Rochester, Rochester, New York 14623, USA

(Received 12 January 2012; accepted 10 April 2012; published online 18 May 2012)

A new deuterium-tritium (D-T) fusion gamma-to-neutron branching ratio [ ${}^3\text{H}(\text{d},\gamma){}^5\text{He}/{}^3\text{H}(\text{d},\text{n}){}^4\text{He}$ ] value of  $(4.2 \pm 2.0) \times 10^{-5}$  was recently reported by this group [Y. Kim *et al.* Phys. Rev. C (submitted)]. This measurement, conducted at the OMEGA laser facility located at the University of Rochester, was made for the first time using inertial confinement fusion (ICF) plasmas. Neutron-induced backgrounds are significantly reduced in these experiments as compared to traditional beam-target accelerator-based experiments due to the short pulse nature of ICF implosions and the use of gas Cherenkov  $\gamma$ -ray detectors with fast temporal responses and inherent energy thresholds. It is expected that this ICF-based measurement will help resolve the large and long-standing inconsistencies in previously reported accelerator-based values, which vary by a factor of approximately 30. The reported value at ICF conditions was determined by averaging the results of two methods: (1) a direct measurement of ICF D-T  $\gamma$ -ray and neutron emissions using absolutely calibrated detectors and (2) a separate cross-calibration against the better known D- ${}^3\text{He}$  gamma-to-proton branching ratio [ ${}^3\text{He}(\text{d},\gamma){}^5\text{Li}/{}^3\text{He}(\text{d},\text{p}){}^4\text{He}$ ]. Here we include a detailed explanation of these results, and introduce as a corroborative method an *in-situ*  $\gamma$ -ray detector calibration using neutron-induced  $\gamma$ -rays. Also, by extending the established techniques to two additional series of implosions with significantly different ion temperatures, we test the branching ratio dependence on ion temperature. The data show a D-T branching ratio is nearly constant over the temperature range 2–9 keV. These studies motivate further investigation into the  ${}^5\text{He}$  and  ${}^5\text{Li}$  systems resulting from D-T and D- ${}^3\text{He}$  fusion, respectively, and result in improved ICF  $\gamma$ -ray reaction history diagnosis at the National Ignition Facility. © 2012 American Institute of Physics. [<http://dx.doi.org/10.1063/1.4718291>]

## I. INTRODUCTION

Understanding the fusion of deuterium (D) and tritium (T) is fundamental to nuclear and plasma physics alike. D-T fusion produces an excited  ${}^5\text{He}$  nucleus, which de-excites via at least three branches,<sup>2</sup>



The most common mode results in the emission of a 3.5 MeV alpha particle and a 14.1 MeV neutron [Eq. (1)]. Less

frequent modes involve the excited  ${}^5\text{He}$  nucleus relaxing to the ground state via the emission of a 16.75 MeV  $\gamma$ -ray,  $\gamma_0$  [Eq. (2)] or to the 1st excited state via emission of a broad  $\gamma$ -ray line at approximately 13.5 MeV,  $\gamma_1$  [Eq. (3)].<sup>3</sup> While  $\gamma_0$  has been measured directly in beam-target experiments,  $\gamma_1$  has been more elusive due in part to the 14.1 MeV neutron background present in such experiments.<sup>4–6</sup>

The D-T gamma-to-neutron branching ratio [ ${}^3\text{H}(\text{d},\gamma){}^5\text{He}/{}^3\text{H}(\text{d},\text{n}){}^4\text{He}$ ] has been measured via accelerator-based beam-target experiments several times in the past.<sup>4–11</sup> In 1963, Buss *et al.*<sup>7</sup> measured  ${}^3\text{H}(\text{d},\gamma){}^5\text{He}$  at deuteron energies ( $E_d$ ) in the range of 150 keV–1.3 MeV, and determined the absolute  ${}^3\text{H}(\text{d},\gamma){}^5\text{He}$  cross-section by cross-calibration against a  ${}^3\text{H}(\text{p},\gamma)$  measurement. The experiments showed that D-T branching ratio increased with  $E_d$ , ranging from  $1.0 \times 10^{-5}$  at  $E_d = 150 \text{ keV}$  to  $3.0 \times 10^{-4}$  at  $E_d = 1.3 \text{ MeV}$ . Other values have also been reported:  $2.3 \times 10^{-5}$  at

<sup>a)</sup>Paper N13 6, Bull. Am. Phys. Soc. 56, 186 (2011).

<sup>b)</sup>Invited speaker.

$E_d = 1$  MeV via a time-of-flight method by Kosiara *et al.*;<sup>8</sup>  $(5.4 \pm 1.3) \times 10^{-5}$  including  $\gamma_0$  only by Cecil *et al.*;<sup>4</sup> and Morgan *et al.*<sup>5</sup> reported a value of  $(5.6 \pm 0.6) \times 10^{-5}$  in the deuteron energy interval from 0 to 275 keV with the assumption that the gamma-ray energies from 13.5 to above 16.7 MeV did not contain any contribution from  $\gamma_1$ . More recently, Kammeraad *et al.*<sup>6</sup> reported a D-T branching ratio of  $(1.2 \pm 0.3) \times 10^{-4}$  using a D-<sup>3</sup>He cross-calibration at  $E_d = 100$  keV and including both  $\gamma_0$  and  $\gamma_1$  in the analysis. This resulted in a value that is 10 times greater than that of Buss, but comparable to Cecil and Morgan after adjustment for the incorporation of  $\gamma_1$ . The disparity in these data can likely be explained by (1) an undetermined D-T fusion  $\gamma$ -ray energy spectrum, and (2) an intractable 14.1 MeV neutron-induced  $\gamma$ -ray background, produced by solid targets in beam-target experiments.

At the OMEGA laser facility, we have developed a new approach to determine the D-T branching ratio under inertial confinement fusion (ICF) plasma conditions in which the effective deuteron beam energy of 14–24 keV is lower than in previous accelerator-based experiments. The recently reported D-T branching ratio of  $(4.2 \pm 2.0) \times 10^{-5}$  (Ref. 1) was obtained by averaging the results of two methods: (1) a direct measurement of ICF D-T  $\gamma$ -ray and neutron emissions using absolutely calibrated detectors and (2) a separate cross-calibration against the better known D-<sup>3</sup>He gamma-to-proton branching ratio [<sup>3</sup>He(d,  $\gamma$ )<sup>5</sup>Li/<sup>3</sup>He(d,p)<sup>4</sup>He]. Neutron-induced backgrounds are significantly reduced as compared to traditional beam-target accelerator-based experiments because of the short pulse nature of ICF implosions, and the use of gas Cherenkov  $\gamma$ -ray detectors with fast temporal responses and inherent energy thresholds. It is expected that this ICF-based measurement will help resolve the large and long-standing variance in previously reported accelerator-based values, which vary by a factor of approximately 30. These ICF-based methods are described in detail below.

To further confirm the reported value for the D-T branching ratio, we now report on an *in-situ*  $\gamma$ -ray detector calibration using neutron-induced  $\gamma$ -rays, and a test of the dependence on ion temperature. The *in-situ* calibration is accomplished by measuring  $\gamma$ -rays generated by the interaction of fusion neutrons with materials (in puck form) intentionally placed in front of  $\gamma$ -ray detectors. The influence of ion temperatures on the D-T branching ratio is examined by using two additional series of implosions, one with a thin glass capsule, and the other with cryogenic fuel in a plastic capsule. The results show that the D-T branching ratio is nearly constant over the temperature range 2–9 keV (11–29 keV effective deuteron beam energy).

This measurement of the D-T branching ratio in an ICF environment is significant to both experimental and theoretical plasma and nuclear physics. Experimentally, a precise value of the D-T gamma-to-neutron branching ratio determined under ICF conditions is a key to understanding fusion reaction history at the National Ignition Facility (NIF). Theoretically, the measurement tests the expectation that the branching ratio is constant at low energies due to the dominance of the  $3/2^+$  resonance transition, and should therefore agree with the results of low-energy beam-target experi-

ments. Finally, it provides branching-ratio data under similar conditions for the mirror processes <sup>3</sup>H(d, $\gamma$ )<sup>5</sup>He and <sup>3</sup>He(d, $\gamma$ )<sup>5</sup>Li, and hence a means to test assumptions about charge symmetry of strong forces in these  $A = 5$  systems.

## II. FUSION $\gamma$ -RAY DETECTION AT OMEGA

ICF implosions at the University of Rochester OMEGA Laser Facility provide a pulsed D-T fusion  $\gamma$ -ray spectrum. To achieve the implosions examined in this work, 60 laser beams (351 nm), with a total energy of 23–28 kJ, were focused on the target at chamber center (TCC) for a duration of 1 ns. For the D-T experiments, the target was a CH plastic shell of thickness 15–30  $\mu$ m and an outer diameter of approximately 1 mm, filled with 15 atm of gaseous D-T fuel in a ratio of D/T  $\sim$  65/35. Application of tera-watts laser power onto the spherical target shell causes the outer part of the shell to heat up and ionize immediately. As the outer part of the shell blasts off, the inner part is accelerated toward the center of the sphere as a consequence of momentum conservation. As a result, the gaseous D-T fuel is compressed, ionized, and heated up to thermonuclear fusion temperature (approximately 10 keV).<sup>12</sup> In ICF plasmas at thermal-equilibrium, most of the nuclear reactions occur at Gamow peak energy on the order of few 10s keV, a value lower than the deuteron beam energies previously reported from beam-target experiments. D-T fusion reactions occur until the compressed fuel disassembles (on the order of 100 ps). D-T implosions at OMEGA typically produce on the order of  $10^{12}$ – $10^{14}$  14.1 MeV fusion neutrons in each shot. A single shot ICF experiment has advantage in D-T branching ratio measurement. Undesired neutron-induced backgrounds can be eliminated through high-bandwidth electronics, which allowed D-T fusion  $\gamma$ -rays to be detected before 14.1 MeV neutrons had a chance to interact with any mass surrounding the target, including the detectors themselves.

Neutron-induced  $\gamma$ -ray ( $n$ - $\gamma$ ) backgrounds from the target are either negligible or can be excluded from the signal using energy thresholds. Because the fuel is gaseous and the capsule wall is thin, implosion areal density remains low and  $n$ - $\gamma$  backgrounds from the target itself are greatly reduced. Known high-energy  $n$ - $\gamma$  backgrounds include those emitted from the inelastic scattering in the shell (<sup>12</sup>C( $n$ , $n'$ ) $\gamma$ ) at 4.44 MeV (Ref. 13)) and from radiative capture in the fuel (D( $n$ , $\gamma$ ) at 15.58 MeV (Ref. 14)). The intensity of the D( $n$ ,  $\gamma$ )  $\gamma$ -ray signal depends on fuel  $\rho R$  (the radial integral of the fuel mass density, whose value from simulation is in the range of 6–8 mg/cm<sup>2</sup>), and is estimated to contribute <0.1% for these non-cryogenic gas-filled capsules at OMEGA. Existing  $n$ - $\gamma$  data for <sup>12</sup>C indicate that the <sup>12</sup>C( $n$ ,  $n'$ ) $\gamma$  reaction has approximately 4 orders of magnitude greater intensity than other  $\gamma$ -ray producing channels in <sup>12</sup>C.<sup>15</sup> Given these data, and the limited areal density of <sup>12</sup>C in the compressed plastic capsules (approximately 40 mg/cm<sup>2</sup> at OMEGA), only the 4.44 MeV  $\gamma$ -ray is significant. This background, though significant, is discriminated using energy thresholds inherent to Cherenkov  $\gamma$ -ray detectors.

Los Alamos National Laboratory (LANL) has developed both gas Cherenkov detector (GCD) (Refs. 16–18) and gamma reaction history (GRH) diagnostics<sup>19,20</sup> in collaboration with

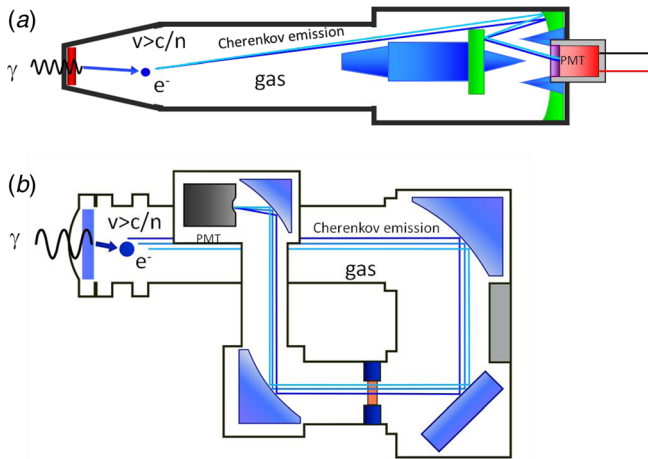


FIG. 1. Schematic cutaway view of (a) GCD and (b) GRH fielded at OMEGA. GCD is inserted into an OMEGA TIM (10 in. manipulator) and placed at 20 cm from TCC. As a prototype to NIF GRH-6m, GRH is attached to the outside of the OMEGA chamber. GRH converter front distance is 187 cm from TCC.

Atomic Weapons Establishment (AWE), Lawrence Livermore National Laboratory (LLNL), and National Security Technologies (NSTec). Figure 1 shows a cutaway view of the detectors, GCD in panel (a) and GRH in panel (b). GCD converts  $\gamma$ -rays to Compton electrons as they interact with a 1.5-cm-thick, 7-cm-diameter beryllium disk. Pressurized  $\text{CO}_2$  (variable up to 100 psia) acts as the dielectric medium, producing optical Cherenkov light above threshold which is then relayed via Cassegranian optics to a Photech ultra-fast, microchannel-plate photo-multiplier tube (PMT). The length of GCD from the beryllium converter to the PMT is about 1 m, and a block of tungsten placed in front of the optics shields  $\gamma$ -rays from reaching the PMT directly. The coaxial design allows GCD to be inserted into the target chamber so as to capture large solid angle. GCD has been fielded at OMEGA since 1999. GRH operates in a similar way as GCD, but with a 1.0-cm-thick, 12.7 cm diameter Al converter, and  $\text{SF}_6$  (up to 200 psia) as the dielectric medium. The optical system relies on off-axis parabolic mirrors to effectively transfer and demagnify the Cherenkov light onto the PMT. This design is mounted outside the target chamber at a distance of 187 cm. GRH has been fielded at OMEGA since 2009, and is the single-channel prototype to the NIF GRH-6m detector. To isolate D-T fusion  $\gamma$ -rays from

the 4.44 MeV  $^{12}\text{C}(n,n'\gamma)$  background,  $\text{CO}_2$  gas pressure in GCD was fixed at 100 psia corresponding to a Cherenkov production energy threshold of 6.3 MeV, while in GRH, the  $\text{SF}_6$  gas pressure was set to 87 psia, corresponding to an energy threshold of 5 MeV.

Figure 2 shows two time traces of the fusion  $\gamma$ -ray signal as detected in (a) GCD, and (b) GRH, where the red traces (shot #54449 and #58162) were taken with Cherenkov gas in the cell and the blue traces (shot #54474 and #58158) without. GCD was installed on an OMEGA Ten Inch Manipulator (TIM) set at a detector-front to TCC distance of 20 cm. In Fig. 2(a), the peak at  $t=23.2$  ns shows the Cherenkov signal resulting from  $\gamma$ -rays emitted during D-T fusion (shot # 54449). Additional peaks after the main peak are the result of impedance-mismatch ringing in the PMT circuit which can be removed by deconvolution using an instrument response function (this was not necessary for this study). When the  $\text{CO}_2$  gas was removed from the gas cell (shot #54474) the Cherenkov peak disappeared, indicating that the signals originate in the gas. After subtracting the “no gas” shot signal (shot #54474) from the D-T  $\gamma$ -rays (shot # 54449), and integrating the resultant time-trace, we can obtain a time-integrated GCD signal in units of nVs. Figure 2(b) shows time traces of Cherenkov signals in the gas-filled GRH (shot # 58162).

Figure 3 shows the time-integrated (a) GCD and (b) GRH  $\gamma$ -ray signals obtained from a total of 22 OMEGA shots taken between 2008 and 2011, where the normalization accounts for differences in PMT quantum efficiency and gain as a function of absolute neutron yield. The absolute D-T neutron yield was measured using the neutron time-of-flight (nTOF-12m) OMEGA facility diagnostic<sup>21</sup> to an uncertainty of less than 5%. The time-integrated  $\gamma$ -ray signal  $S_{\gamma}^{DT}(E_{thr})$  in units of volt-seconds (Vs) results from the detector response  $R(E; E_{thr})$  to the D-T fusion  $\gamma$ -ray yield  $Y_{\gamma}^{DT}$  and an assumed D-T fusion  $\gamma$ -ray spectrum  $I_{\gamma}^{DT}(E)$  (normalized to one) at a given energy threshold  $E_{thr}$ . It can be written

$$\begin{aligned}
 S_{\gamma}^{DT}(E_{thr}) &= Y_{\gamma}^{DT} \int_{E_{thr}}^{\infty} I_{\gamma}^{DT}(E) R(E; E_{thr}) dE \\
 &= Y_n^{DT} B_{\gamma/n}^{DT} (\Delta\Omega/4\pi) QGer \int_{E_{thr}}^{\infty} I_{\gamma}^{DT}(E) R'(E; E_{thr}) dE,
 \end{aligned}
 \tag{4}$$

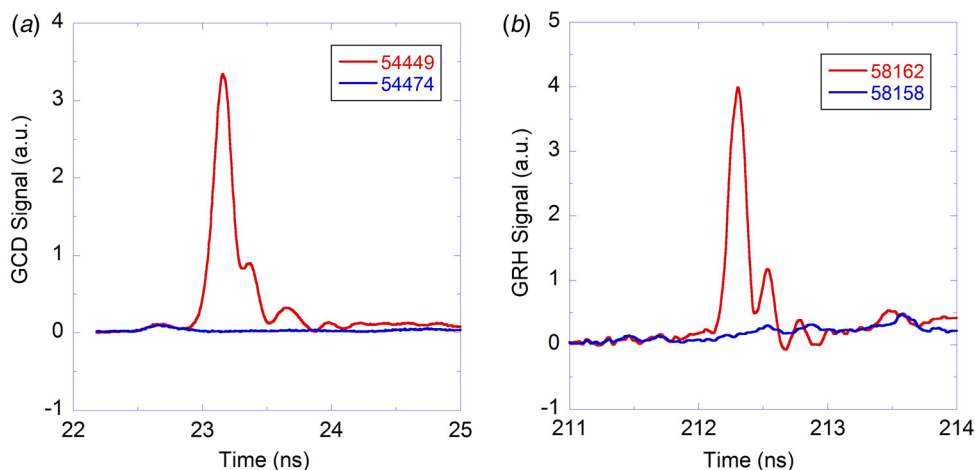


FIG. 2. Time history of D-T fusion  $\gamma$ -rays measured from (a) GCD, where shot 54 449 was taken at 100 psia of  $\text{CO}_2$  and shot 54 474 was taken without gas, (b) GRH, where shot 58 162 was taken at  $\text{SF}_6$  87 psia and shot 58 158 was taken without gas. Absolute time bases are arbitrary.

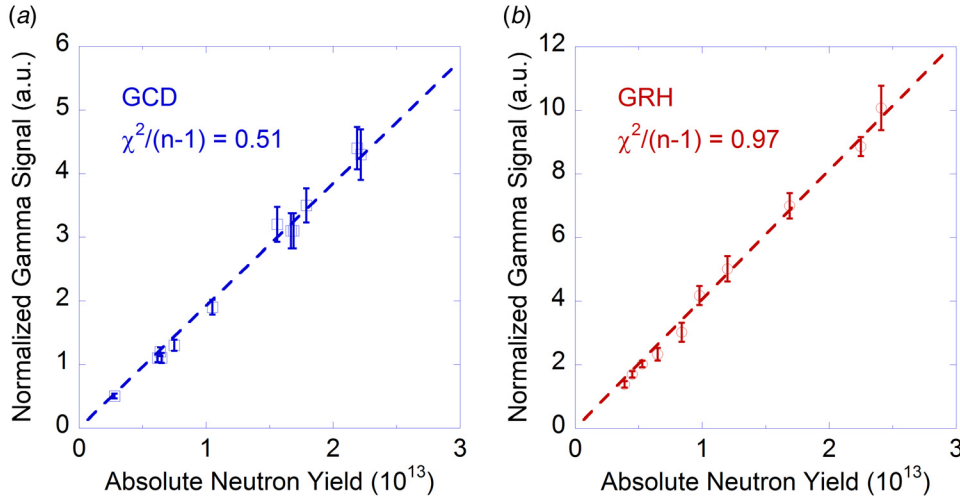


FIG. 3. Time-integrated and normalized (a) GCD and (b) GRH  $\gamma$ -ray signals ( $S_{\gamma}^{DT}(E_{thr})$ ) as a function of absolute neutron yield, obtained from 22 OMEGA shots.  $S_{\gamma}^{DT}(E_{thr})$  increases linearly with neutron yield, indicating constant gamma-to-neutron branching ratio.

where  $Y_n^{DT}$  is the measured neutron yield,  $B_{\gamma/n}^{DT} = Y_{\gamma}^{DT}/Y_n^{DT}$  is the D-T branching ratio,  $\Delta\Omega/4\pi$  is the solid angle fraction of the converter plate (GCD's  $\Delta\Omega/4\pi = 1.1 \times 10^{-2}$  and GRH's  $\Delta\Omega/4\pi = 2.9 \times 10^{-4}$ ),  $Q$  is the PMT quantum efficiency to the UV/visible Cherenkov emission spectrum which reaches the PMT photocathode (typically 15%),  $G$  is the PMT gain (typically  $10^4$ – $10^6$ ),  $e = 1.602 \times 10^{-19}$  C is the charge of an electron, and  $r = 50 \Omega$  is the circuit resistance.  $R'(E; E_{thr})$  is the response of the Cherenkov gas cell to  $\gamma$ -rays of energy  $E$  in units of productive Cherenkov photons/incident  $\gamma$ -ray. Thus, the normalized  $\gamma$ -ray signal  $S_{\gamma}^{DT}(E_{thr}) = S_{\gamma}^{DT}(E_{thr})/(QGe r \Delta\Omega/4\pi)$  is proportional to  $Y_n^{DT}$ .

In Figure 3, it can be seen that normalized  $\gamma$ -ray signals from GCD and GRH do indeed increase linearly with neutron yield. Random uncertainty in time-integrated signals comes from two main contributions: uncertainty in defining the signal integration period and Poisson statistical noise. The Poisson noise is estimated by the number of detected  $\gamma$ -rays ( $N_{\gamma}$ ). Using the simulated detector efficiency (to be explained in Sec. III A in detail) and measured signal level, it is estimated that there are approximately 2000  $\gamma$ -rays detected by GCD at a neutron yield of  $3 \times 10^{12}$ , the lowest yield in these GCD experiments. Fractional Poisson noise uncertainty is  $1/\sqrt{N_{\gamma}}$  and less than 2% for all GCD experiments. GRH collected data at a minimum neutron yield of  $4 \times 10^{12}$ , where approximately 8% Poisson noise is estimated. Two signal integration methods are used. The first method is to integrate signal up to the third PMT ring (24.1 ns in Fig. 2(a), 213.2 ns in Fig. 2(b)). Second method is Gaussian integration of the main peak only, which is then multiplied by a factor of 1.5, which was pre-determined by separate PMT impulse tests. GCD's uncertainty in signal integration is less than 9% and GRH is less than 7%. In summary, quadrature sum of random uncertainty is less than 12% for GCD and less than 11% for GRH (plotted as error bars in Fig. 3). Given random uncertainty, reduced chi-squared is smaller than 1 for both detectors. Inverting Eq. (4),  $B_{\gamma/n}^{DT}$  can be inferred from the expression

$$B_{\gamma/n}^{DT} = \frac{S_{\gamma}^{DT}(E_{thr})/Y_n^{DT}}{\int_{E_{thr}}^{\infty} I_{\gamma}^{DT}(E)R'(E; E_{thr})dE}. \quad (5)$$

The spectral shapes of the  $\gamma_1$  and  $\gamma_0$  lines have been determined using an R-matrix analysis.<sup>3,22</sup> The ratio of these lines ( $\gamma_1/\gamma_0$ ) has been experimentally determined to be in the range of 2-3 based on Cherenkov energy-thresholding scans also conducted at OMEGA with GCD.<sup>23</sup> This information is used to determine  $I_{\gamma}^{DT}(E)$  which will be reported in detail separately.

### III. REVIEW OF D-T BRANCHING RATIO MEASUREMENT

To determine the D-T branching ratio under ICF implosion conditions, we have developed two methods. The first method utilizes absolute calibrations for  $\gamma$ -ray and neutron measurements achieved through Monte Carlo simulations and direct measurements at the high-intensity gamma-ray source (HI $\gamma$ S). The second method relies on cross-calibration to the better known D-<sup>3</sup>He gamma-to-proton branching ratio. Based on a weighted average of the two methods, we arrived at a D-T gamma-to-neutron branching ratio of  $(4.2 \pm 2.0) \times 10^{-5}$ .<sup>1</sup>

#### A. The D-T branching ratio via absolute calibration at HI $\gamma$ S

An absolute determination of  $B_{\gamma/n}^{DT}$ , requires accurate GCD and GRH responses  $R'(E; E_{thr})$ . The two detector responses have been calculated using Monte Carlo particle transport simulations. The detector models were developed using the ACCEPT code, an integrated tiger series Monte Carlo code written by Sandia National Laboratory.<sup>24</sup> ACCEPT simulates high energy photon/electron transport in 3-dimensions. The production and generalized ray trace of Cherenkov radiation has been incorporated into ACCEPT. Directionality is given by the Cherenkov relation

$$\cos\theta = \frac{1}{\beta n(\lambda)}, \quad (6)$$

where  $\theta$  is the Cherenkov emission angle relative to the electron direction,  $\beta$  is the ratio of electron speed in the medium to the speed of light in vacuum ( $v_e/c$ ), and  $n(\lambda)$  is the material refractive index at wavelength  $\lambda$ .<sup>25</sup> The number of

Cherenkov photons emitted along an electron path length ( $dN/dl$ ) is given by

$$\frac{dN}{dl} = 2\pi\alpha \int_{\lambda_1}^{\lambda_2} \left\{ 1 - \frac{1}{\beta^2 n^2(\lambda)} \right\} \frac{d\lambda}{\lambda^2}, \quad (\lambda_2 > \lambda_1), \quad (7)$$

within a spectral region defined by wavelengths  $\lambda_1$  and  $\lambda_2$ , and  $\alpha$  is the fine-structure constant ( $=1/137$ ). Recently, complementary work has been added to this study using GEANT4, a three-dimensional particle physics code developed by contributing groups, such as CERN and SLAC.

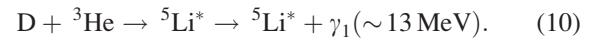
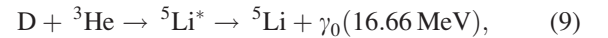
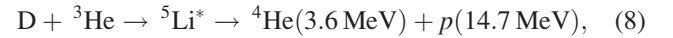
Both simulation codes (ACCEPT and GEANT4) have been validated against measurements at the HI $\gamma$ S operated by the Triangle Universities Nuclear Laboratory (TUNL) on the Duke University Campus.<sup>26</sup> The HI $\gamma$ S provided a well characterized, 1 cm diameter disk beam of  $\gamma$ -rays pulsed at 5.6 MHz at flux levels of several  $10^7$  gammas/s and three different beam energies (4.4, 10.0, and 16.86 MeV). Scans were performed in beam position and Cherenkov threshold energy (i.e., gas pressure) for 2 different gases (CO<sub>2</sub> and SF<sub>6</sub>). Measurements were performed in both a time-integrated, current mode using Keithley electrometers and, in a temporally resolved, single-photon counting mode using 12.5 GHz Tektronix DPO71254 scopes in FastFrame mode. Figure 4(a) shows measured GCD response in units of number of Cherenkov photon per incident  $\gamma$ -ray as a function of CO<sub>2</sub> gas pressure, where inlet  $\gamma$ -ray energy was fixed at 16.86 MeV. It can be seen that GCD response increased as CO<sub>2</sub> gas pressure increases as expected. GEANT4 results follow the GCD response at various CO<sub>2</sub> pressures, however, the simulation is consistently higher than measurement. A factor of approximately 0.7 allows the GCD model to match the measurement. Figure 4(b) shows measured GRH response as a function of SF<sub>6</sub> pressure at fixed 4.4 MeV HI $\gamma$ S  $\gamma$ -ray energy. ACCEPT simulation also requires a factor of approximately 0.7 to be applied to the GRH model.

Keeping a correction factor of 0.7, the simulations were then extended to the OMEGA configuration in which an isotropic  $\gamma$ -ray source shines on GCD front-face placed 20 cm from TCC, and GRH front-face placed 187 cm from TCC. These simulations were used to compute the absolute detector response  $R'(E; E_{thr})$  for each of the detectors. Figure 5 shows that D-T branching ratios obtained from GCD (blue)

and from GRH (red) based on these responses are in agreement. An absolute D-T branching ratio of  $(4.3 \pm 1.8) \times 10^{-5}$  with 7.3% random uncertainty and 33.9% systematic uncertainty is inferred by a weighted average of the results from the two detectors. The main sources of systematic uncertainty are: 30% in simulated response, 10% in PMT quantum efficiency, and 10% in PMT gain.

## B. The D-T branching ratio via D-<sup>3</sup>He cross-calibration at OMEGA

To lessen the possibility of unknown systematic uncertainties in the absolute method, the D-<sup>3</sup>He cross-calibration method used by Kosiara<sup>8</sup> and Kammeraad<sup>6</sup> was adopted. D-<sup>3</sup>He fusion is similar to D-T fusion [Eqs. (1)–(3)] with the exception that <sup>5</sup>He\* is replaced with its mirror nucleus, <sup>5</sup>Li\*



The energy level structures of <sup>5</sup>He\* and <sup>5</sup>Li\* are very close to each other, and thus their  $\gamma$ -ray energy spectra are similar.<sup>6</sup> The D-T neutron emission is replaced by a 14.7 MeV proton in the D-<sup>3</sup>He reaction [Eq. (8)], further reducing problems associated with the 14.1 MeV neutron backgrounds found in beam-target D-T  $\gamma/n$  branching ratio experiments. During the D-<sup>3</sup>He implosion D-D reactions generate 23.8 MeV  $\gamma$ -rays, 2.45 MeV neutrons, and tritium as well. If the secondary tritium fuses with deuterium fuel, D-T  $\gamma$ -rays may contribute to Cherenkov signals. To test potential unwanted background signal, we have imploded pure D<sub>2</sub> capsules and recorded  $\gamma$ -ray signals with the same GCD instrument. Gamma-ray signal levels from the pure D<sub>2</sub> capsules were less than 1% of that of D-<sup>3</sup>He implosions. 14.7 MeV proton-induced background  $\gamma$ -rays (e.g., (p,p' $\gamma$ ), (p, $\gamma$ )) are also estimated to negligible based on published cross-sections and the approximately 10 mg/cm<sup>2</sup> glass capsule areal density achieved in these implosions. Assuming the  $\gamma$ -ray spectra are identical for <sup>5</sup>He\* and <sup>5</sup>Li\*, and without knowing the absolute detector response  $R'(E; E_{thr})$ , we can infer  $B_{\gamma/n}^{DT}$  as,

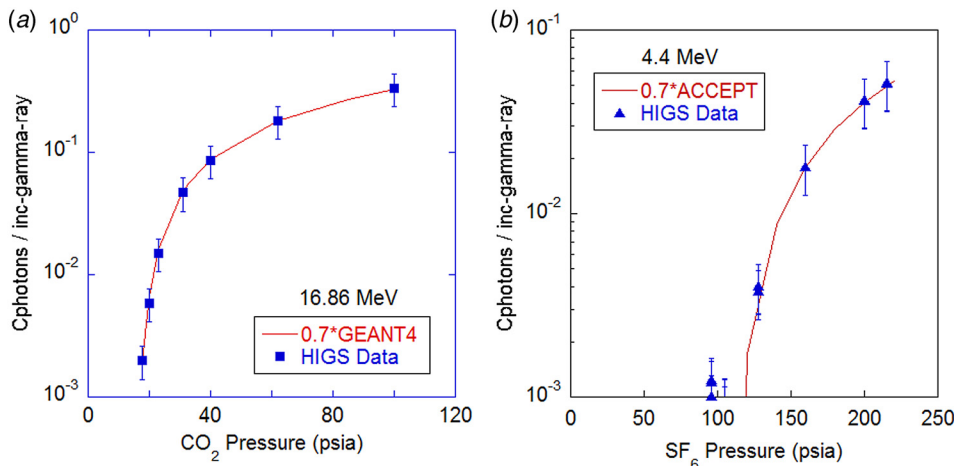


FIG. 4. (a) Comparison of GEANT4 simulation and GCD measurement at HI $\gamma$ S, where fixed 16.86 MeV 1 cm diameter  $\gamma$ -ray beam and varied CO<sub>2</sub> pressure up to 100 psia are used. (b) Comparison of ACCEPT simulation and GRH measurement at HI $\gamma$ S, where 4.4 MeV  $\gamma$ -ray beam was injected to GRH front at center on axis and SF<sub>6</sub> pressure was varied up to 220 psia.

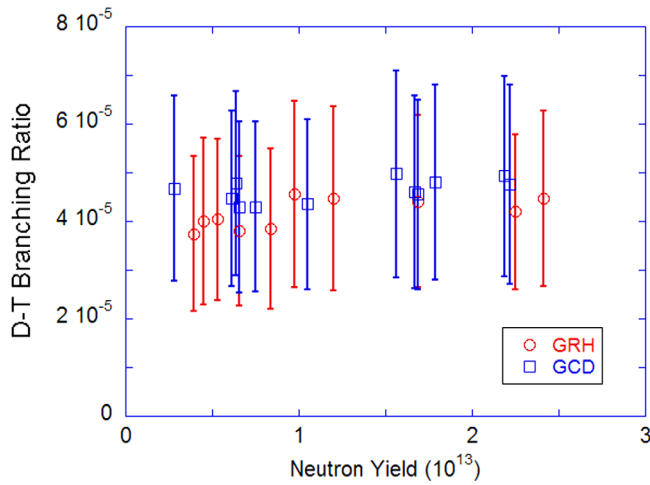


FIG. 5. D-T branching ratios determined from GCD (blue) and from GRH (red) are in agreement. After a weighted average, a D-T branching ratio of  $(4.3 \pm 1.8) \times 10^{-5}$  is obtained from absolute calibration method.

$$B_{\gamma/n}^{DT} = B_{\gamma/p}^{D^3He} \frac{S_{\gamma}^{DT}(E_{thr})/Y_n^{DT}}{S_{\gamma}^{D^3He}(E_{thr})/Y_n^{D^3He}}. \quad (11)$$

D-<sup>3</sup>He and D-T implosion experiments were performed on the same shot day at OMEGA, over two shot campaigns (September 2010 and May 2011). The D-<sup>3</sup>He capsules were glass, and filled with 6 atm of D<sub>2</sub> and 12 atm of <sup>3</sup>He. Gamma-ray measurements were made on both types of implosions with the same GCD instrument. Neutron yield measurements were made for the D-T implosions as before, while proton yield measurements were made for the D-<sup>3</sup>He implosions. In contrast to the neutron yield measurements, proton yield measurements in ICF implosions need to account for particle flux anisotropy which is caused by electromagnetic fields generated around the capsule during implosion.<sup>27</sup> These field effects deflect charged fusion products and lead to variation in yield measurements taken around the chamber on the order of approximately 10%. To reduce uncertainty, charged particle yield diagnostics were fielded at multiple angles around target chamber center from which a weighted average of the yield was taken based on the solid angle covered by each detector. For the September 2010 shot campaign, six proton yield diagnostics were fielded at multi-

ple positions around the target chamber. These included two charged particle spectrometers (CPS1 and CPS2), three wedge range filters (WRFs) fielded on TIM 2, and the magnetic recoil spectrometer (MRS) in the charged particle configuration.<sup>28</sup> In all cases, the field effect induced variation in particle flux was greater than the variation from statistical uncertainty; therefore, the measurement uncertainty was taken as the weighted standard deviation of the individual yield measurements. For the September 2010 shot campaign, this gave measurement uncertainties between 7.8 and 11.2% with an average uncertainty of 9.1%. For the May 2011 shot campaign, five additional proton yield diagnostics were fielded for improved averaging of field effect variation and reduced measurement uncertainty. In addition, range filters (RFs) were used in place of WRFs to provide greater solid angle coverage and more accurate yield measurement under high particle fluence. The complete proton diagnostic suite included CPS1 and CPS2, three RFs fielded on TIM 2, three RFs on TIM 4, two RFs on TIM 6, and MRS in the charged particle configuration. For the May 2011 shot campaign, this gave measurement uncertainties between 3.6% and 11.0% with an average uncertainty of 6.7%.

Gamma-ray signals from D-T and D-<sup>3</sup>He, measured with the same GCD setup and analyzed with the same signal integration scheme, were then combined with the proton yield values for D-<sup>3</sup>He and the neutron yield values for D-T. Figure 6 shows (a) September 2010 and (b) May 2011 GCD reaction histories for D-<sup>3</sup>He (blue) and D-T (red) implosions normalized for proton and neutron yields, respectively. Data in Figure 6(a) were measured using a double-stage PMT (210-21080605), while another double-stage PMT (210-22091009) was used in Figure 6(b). Integrating the signals from D-<sup>3</sup>He and D-T shots, we obtain  $\frac{S_{\gamma}^{DT}(E_{thr})/Y_n^{DT}}{S_{\gamma}^{D^3He}(E_{thr})/Y_p^{D^3He}} = \frac{B_{\gamma/n}^{DT}}{B_{\gamma/p}^{D^3He}} = (0.39 \pm 0.09)$  from Figure 6(a) and  $(0.26 \pm 0.07)$  from Figure 6(b), respectively. Average of two shot days gives us  $\frac{B_{\gamma/n}^{DT}}{B_{\gamma/p}^{D^3He}} = (0.31 \pm 0.08)$ . Applying the published value of total (i.e.,  $\gamma_0 + \gamma_1$ )  $B_{\gamma/p}^{D^3He} = (12.5 \pm 4.2) \times 10^{-5}$  from Cecil *et al.*<sup>29</sup> to this data, results in a D-T branching ratio of  $B_{\gamma/n}^{DT} = (3.9 \pm 2.3) \times 10^{-5}$  for the cross-calibration approach, where random uncertainty is 25.4% and systematic uncertainty is 33.6%.

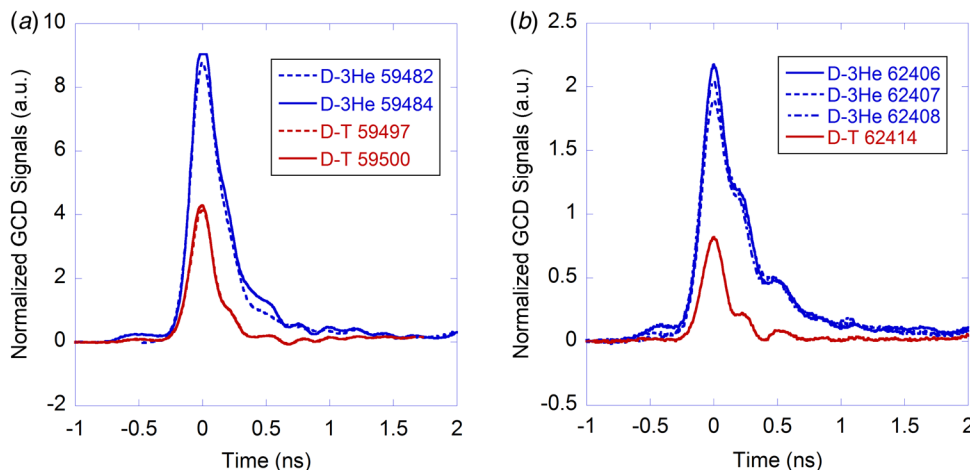


FIG. 6. GCD reaction histories from (a) September 2010 and (b) May 2011, where top curves (blue) show D-<sup>3</sup>He  $\gamma$ -ray signals normalized by proton yields and bottom curves (red) show D-T  $\gamma$ -ray signals normalized by neutron yields. D-T  $\gamma/n$  branching ratio is determined to be  $(0.31 \pm 0.08)$  of the D-<sup>3</sup>He  $\gamma/p$  branching ratio from the average of two show days.

TABLE I. Summary of D-T branching ratios determined by two methods.

Calibrations	Branching ratio ( $1 \times 10^{-5}$ )	Statistical uncertainty (%)	Systematic uncertainty (%)
Absolute	$4.3 \pm 1.8$	7.3	33.9
D- <sup>3</sup> He	$3.9 \pm 2.3$	25.4	33.6
Average	$4.2 \pm 2.0$		

### C. Weighted-average D-T branching ratio

A weighted-average value for the D-T branching ratio over the two methods; absolute and D-<sup>3</sup>He cross-calibration, is  $(4.2 \pm 2.0) \times 10^{-5}$  and summarized in Table I. The absolute method depends on systematic uncertainty in PMT parameters (10% in quantum efficiency and 10% in gain) and in detector response simulation (30%). The D-<sup>3</sup>He cross-calibration reduces systematic uncertainty in PMT parameters and removes detector response, however, this method relies on inherent D-<sup>3</sup>He gamma-to-proton branching ratio uncertainty (approximately 34%) and the assumption that the  $\gamma$ -ray spectrum of <sup>5</sup>He and <sup>5</sup>Li are identical.

## IV. SUPPORTING EVIDENCE

### A. The D-T branching ratio via neutron-induced $\gamma$ -ray calibration

To confirm this value for the D-T branching ratio, an additional *in-situ* method based on the measurement of neutron-induced  $\gamma$ -rays has been developed. The calibration relies on the comparison of relative intensities between a D-T  $\gamma$ -ray signal and a  $\gamma$ -ray signal generated by the interaction of fusion neutrons with materials (in puck form) intentionally placed in front of GCD.<sup>30</sup> A schematic of this “puck method” for GCD is shown in Figure 7.

In the puck method, GCD detects  $\gamma$ -rays directly from the D-T implosion, as well as those created by 14.1 MeV fusion neutron-induced inelastic scattering ( $n, n'\gamma$ ) and neutron capture ( $n, \gamma$ ) in the puck. The D-T fusion  $\gamma$ -rays arrive at the detector well before the neutron-induced  $\gamma$ -rays whose time of arrival is constrained by the speed of the 14.1 MeV neutrons (approximately 1/6 of speed of light). For a puck

placed 6 cm from TCC, this arrival-time difference is approximately 1 ns. The neutron-induced  $\gamma$ -ray yield arising from a puck is

$$Y_{\gamma}^{puck} = Y_n^{DT} \frac{\Delta\Omega_{puck}}{4\pi} \frac{\sigma_{puck}}{m_{puck}} \langle \rho R \rangle_{puck} f(\theta), \quad (12)$$

where  $Y_n^{DT}$  is the measured 14.1 MeV neutron yield,  $\sigma_{puck}$  is  $\gamma$ -ray production cross-section,  $m_{puck}$  is mass of the puck material,  $\frac{\Delta\Omega_{puck}}{4\pi} \langle \rho R \rangle_{puck}$  is the solid angle corrected areal density of the puck, and  $f(\theta)$  accounts for the angular dependence of the  $\gamma$ -ray emission from the puck.<sup>31</sup> The time-integrated GCD signal from the neutron-induced puck  $\gamma$ -rays can be expressed as,

$$S_{\gamma}^{puck}(E_{thr}) = Y_{\gamma}^{puck} QGer \int_{E_{thr}}^{\infty} I_{\gamma}^{puck}(E) R'(E; E_{thr}) dE, \quad (13)$$

where  $E_{thr}$  is the energy threshold in the detector (6.3 MeV in this work),  $I_{\gamma}^{puck}$  is neutron-induced  $\gamma$ -ray energy spectrum for the particular puck material (area normalized to one), and  $R'(E; E_{thr})$  is the detector response calculated using Monte-Carlo codes. The D-T branching ratio can then be expressed in terms of the relative intensity of the D-T  $\gamma$ -ray signal to the puck  $\gamma$ -ray signal. From Eqs. (4) and (13),

$$B_{\gamma/n}^{DT} = Y_{\gamma}^{puck} \cdot \left\{ \frac{S_{\gamma}^{DT}(E_{thr})}{S_{\gamma}^{puck}(E_{thr})} \right\} \cdot \left\{ \frac{\int_{E_{thr}}^{\infty} I_{\gamma}^{puck}(E) R'(E; E_{thr}) dE}{\frac{\Delta\Omega}{4\pi} \int_{E_{thr}}^{\infty} I_{\gamma}^{DT}(E) R'(E; E_{thr}) dE} \right\}. \quad (14)$$

An advantage of this method is that absolute PMT parameters, such as quantum efficiency and gain, cancel in the ratio and so it is no longer necessary to determine their values. Additionally, the uncertainty in the ratio of signals and responses is less than the uncertainty in their absolute values. However, new uncertainties come from the values for  $Y_{\gamma}^{puck}$  and  $I_{\gamma}^{puck}$  as determined from the nuclear data base (ENDF/B-VII).<sup>32</sup> These uncertainties can be relatively large and difficult to estimate and so this technique is used as a corroborating method for determination, and is not used in the final value.

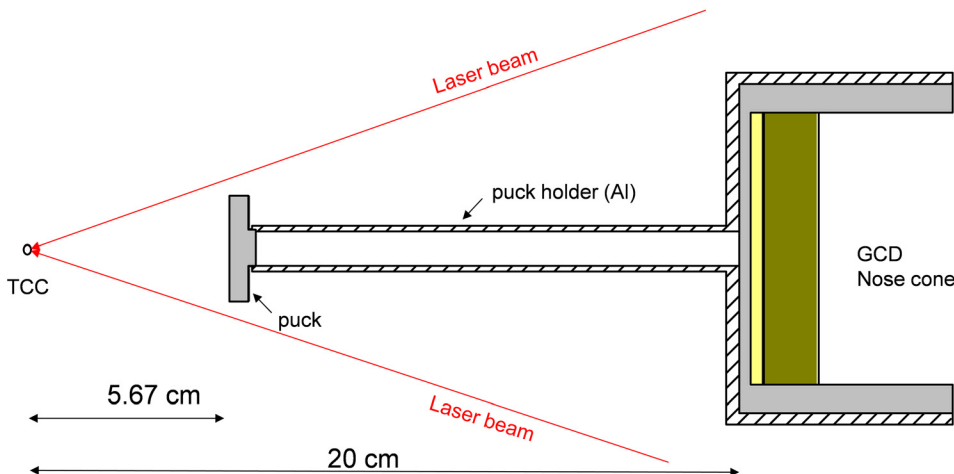


FIG. 7. A schematic drawing of puck experiment at OMEGA (puck used: Si, Cu, Al, and C).



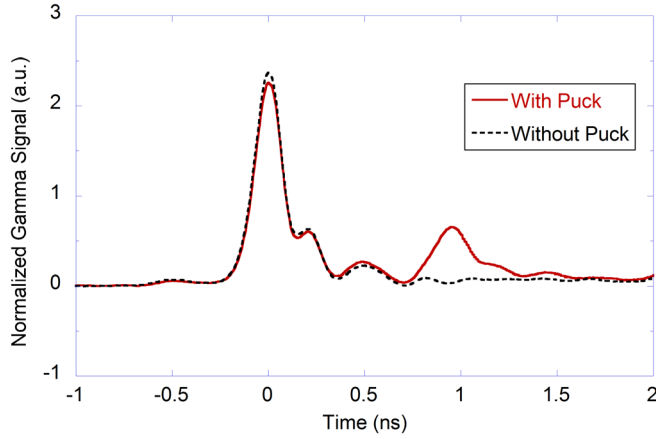


FIG. 8. Simultaneous measurement of D-T fusion  $\gamma$ -rays and 14.1 MeV neutron-induced Si  $\gamma$ -rays.

Two GCD time traces taken at OMEGA are shown in Figure 8, one measurement with a silicon (Si) puck in place (red solid line), and one with no puck (black dotted line). The 0.64 cm thick Si puck has a diameter of 2.54 cm and was placed 5.67 cm from TCC. The high temporal bandwidth of GCD allowed detection of the D-T fusion  $\gamma$ -rays ( $t=0$  ns) along with the time-delayed neutron-induced  $\gamma$ -ray signal originating from the puck ( $t \cong 1$  ns). The time interval between the two signals was found to be 948 ps, a value consistent with the expected time-of-flight difference between the transit times of D-T  $\gamma$ -rays and 14.1 MeV neutrons to the Si puck ( $163 \text{ ps/cm} \times 5.67 \text{ cm} = 924 \text{ ps}$ ). The ratio of the time-integrated Si  $\gamma$ -ray signal to the D-T  $\gamma$ -ray signal,  $\frac{S_{\gamma}^{\text{puck}}(E_{\text{thr}})}{S_{\gamma}^{\text{DT}}(E_{\text{thr}})}$  was 0.31 for the Si puck measurement.

To determine  $Y_{\gamma}^{\text{puck}}$  and  $I_{\gamma}^{\text{puck}}$ , Monte Carlo N-particle transport code (MCNP) with the ENDF/B-VII database was used.<sup>33</sup> The calculation for the geometry fielded is shown in Figure 9. The number of Si  $\gamma$ -rays arriving at the front of GCD as a function of  $\gamma$ -ray energy (red curve) is shown with the  $\gamma$ -ray response function  $R'(E; E_{\text{thr}} = 6.3 \text{ MeV})$  for GCD (black curve). The expected Si puck  $\gamma$ -ray signal intensity,  $Y_{\gamma}^{\text{puck}} \int_{E_{\text{thr}}}^{\infty} I_{\gamma}^{\text{puck}}(E) R'(E; E_{\text{thr}}) dE$ , is determined by folding the GCD response function with the calculated Si neutron-induced  $\gamma$ -ray energy spectrum.

The D-T branching ratio via this puck method was determined by averaging values from four different puck experiments performed at OMEGA. The values are shown in Table II. For three of the experiments (Si, Al and Cu pucks), the measurement was made with GCD at an energy threshold of  $E_{\text{thr}} = 6.3 \text{ MeV}$ . For the graphite (C) puck experiment, the measurement was made with GRH at  $E_{\text{thr}} = 3 \text{ MeV}$ . The appropriate adjustments were made in the calculations, and

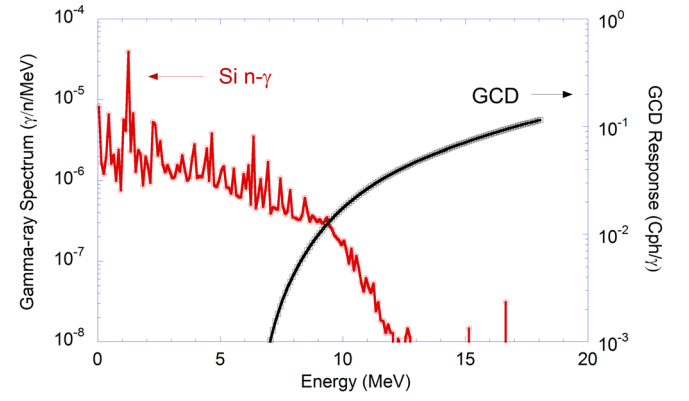


FIG. 9. Simulated Si n- $\gamma$  spectrum using MCNP (red curve on the left) and simulated GCD response using ACCEPT (black curve on the right).

differences in detector settings were eliminated in the ratio, as discussed. Using these data and Eq. (14), we obtained a weight-averaged D-T branching ratio of  $(4.8 \pm 2.6) \times 10^{-5}$ . This value is nearly 15% larger than the D-T branching ratio determined in session III but consistent within the errors of the measurement. In the neutron-induced  $\gamma$ -ray (puck) method, systematic uncertainty in detector response ratio is reduced to 10% and the PMT uncertainties cancel out, however, nuclear cross-section uncertainty (10% in C, 30% in Si and Cu, and 50% in Al) is introduced. In the future, further evaluation of 14.1 MeV neutron-induced differential cross-sections in energy and angle are required to improve accuracy and reduce uncertainty of the puck method.

## B. The influence of ion temperature on the D-T branching ratio

The reported D-T branching ratio value of  $(4.2 \pm 2.0) \times 10^{-5}$  has been determined using capsules made of a thin plastic shell, where burn-averaged ion temperature ( $T_{\text{ion}}$ ) was  $5 \pm 2 \text{ keV}$ . We have extended this technique to two additional series of ICF implosions at OMEGA, having different  $T_{\text{ion}}$ . First, thin-glass ( $\text{SiO}_2$ ) capsules with a thickness in the range of 3.5–4.5  $\mu\text{m}$  were used. In the second case, CH plastic capsules with cryogenically layered D-T fuel were used. The measured D-T branching ratios are shown in Figure 10 as a function of  $T_{\text{ion}}$ . For comparison, the previous plastic results are plotted as well.

Three cryogenically layered D-T implosions produced neutron yield in the range of  $(2.2\text{--}5.5) \times 10^{12}$  and  $T_{\text{ion}}$  in the range of 2–3 keV. D-T branching ratio from the cryogenically layered capsule is  $(5.8 \pm 2.2) \times 10^{-5}$ , which is higher than that of previous D-T plastic signals by nearly 38% but

TABLE II. D-T branching ratio inferred with various puck materials.

Puck	$E_{\text{thr}}$ (MeV)	Detector	$S_{\gamma}^{\text{puck}}/S_{\gamma}^{\text{DT}}$	$Y_{\gamma}^{\text{puck}} \int_{E_{\text{thr}}}^{\infty} I_{\gamma}^{\text{puck}}(E) R'(E; E_{\text{thr}}) dE$ (# photon/source-n)	$\frac{\Delta\Omega}{4\pi} \int_{E_{\text{thr}}}^{\infty} I_{\gamma}^{\text{DT}}(E) R'(E; E_{\text{thr}}) dE$ (# photon/source- $\gamma$ )	Branching ratio ( $\times 10^{-5}$ )
Si	6.3	GCD	0.31	$5.72 \times 10^{-9}$	$4.47 \times 10^{-4}$	$4.1 \pm 1.9$
Al	6.3	GCD	0.11	$3.49 \times 10^{-9}$	$4.47 \times 10^{-4}$	$7.2 \pm 5.2$
Cu	6.3	GCD	0.07	$1.27 \times 10^{-9}$	$4.47 \times 10^{-4}$	$4.0 \pm 1.9$
C	3.0	GRH	0.72	$1.02 \times 10^{-9}$	$2.70 \times 10^{-5}$	$5.18 \pm 1.2$

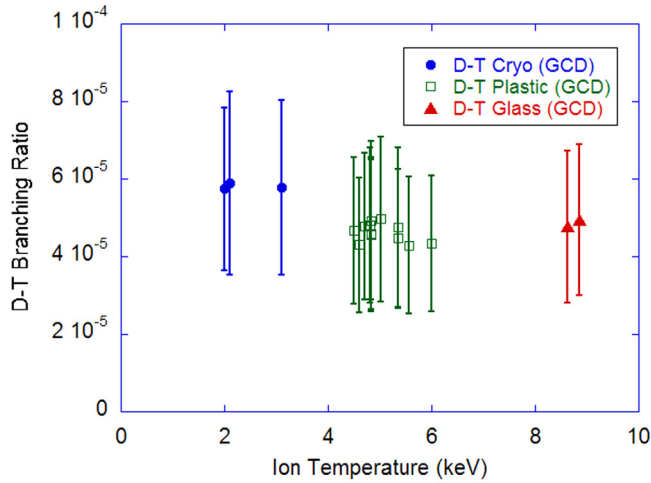


FIG. 10. D-T branching ratios obtained from cryogenic D-T fuel in CH capsules (blue) and D-T glass capsules (red) are compared to the D-T branching ratio of CH capsules (green), showing that no clear temperature dependency on D-T branching ratio within error bars.

consistent with the errors of the measurement. Possible background interference may arise from a radiative capture in the fuel ( $D(n,\gamma)$ ) at 15.58 MeV.<sup>14</sup> The intensity of the  $D(n,\gamma)$  depends on fuel  $\rho R$ , so its contribution to the GCD signal from the high  $\rho R$  cryogenic fuel may help account for higher apparent D-T branching ratio.

Two glass capsule implosions produced high neutron yield in the range of  $(7-8) \times 10^{13}$  and  $T_{ion}$  in the range of 8–9 keV. In contrast to CH plastic capsules, where the 4.44 MeV background  $\gamma$ -rays were successfully isolated from the D-T fusion  $\gamma$ -rays by means of 6.3 MeV energy threshold, the glass capsules produce continuum neutron-induced  $SiO_2$   $\gamma$ -rays, which can easily extend above the 6.3 MeV threshold energy. According to the MCNP simulation (Sec. IV A), background signals from glass capsules contribute less than 3% to the total measured  $\gamma$ -ray signal. With the 3% correction, determined D-T branching ratio from two D-T glass capsule was  $(4.9 \pm 2.0) \times 10^{-5}$ .

## V. DISCUSSION

In ICF plasmas at thermal-equilibrium, most of the nuclear reactions occur at the Gamow peak energy  $E_0$ ; which for a D-T reaction can be written as  $E_0 = 6.66(T_{ion})^{2/3}$ , where  $T_{ion}$  is the burn-averaged ion temperature in units of keV.<sup>34,35</sup> For these OMEGA ICF implosions,  $T_{ion}$  was 2–9 keV, resulting in a center-of-mass  $E_0$  value of 11–29 keV. When translated to beam-target experimental conditions, these values correspond to an effective deuteron beam energy of  $E_d = 18-48$  keV, a value significantly lower than the deuteron beam energies previously reported from beam-target experiments.<sup>4-11</sup> In Figure 11, the D-T branching ratio of  $(4.2 \pm 2.0) \times 10^{-5}$  determined at ICF conditions is compared to earlier beam-target measurements. The horizontal error bar of present data (red closed circle) represents the temperature range of each measurement. The present analysis incorporates the D-T fusion  $\gamma$ -ray emissions,  $\gamma_0$  and  $\gamma_1$ . We used the ratio of these lines ( $\gamma_1/\gamma_0$ ) in the range of 2–3 based on energy-thresholding experiments conducted at

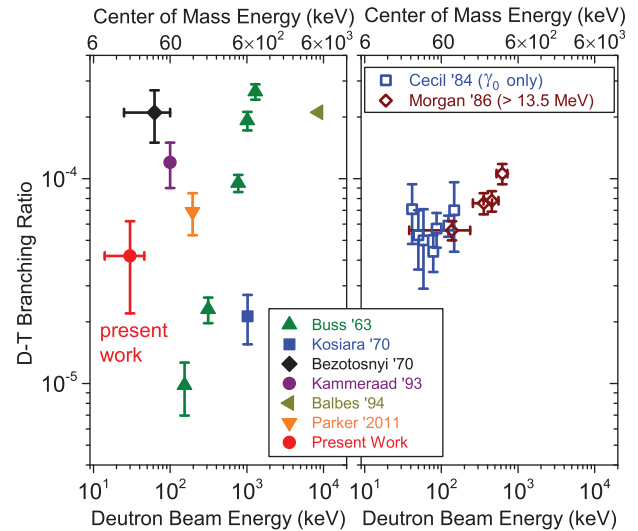


FIG. 11. D-T branching ratio determined from ICF implosion studies is compared to earlier beam-target measurements. Branching ratios shown in the left figure include  $\gamma_0$  and  $\gamma_1$  emissions, while only  $\gamma_0$  is considered in the right figure. The energy band of present ICF data has been extended relative to Ref. 1 by glass and cryo implosions.

OMEGA with GCD.<sup>23</sup> On the right figure, Cecil *et al.*<sup>4</sup> data are plotted where only  $\gamma_0$  is considered and also Morgan *et al.*<sup>5</sup> data are plotted where Morgan *et al.*, assumed that gamma-ray energies from 13.5 to above 16.7 MeV did not contain any contribution from  $\gamma_1$ . In those measurements  $\gamma_1$  was obscured by the 14.1 MeV neutron-induced background.

The dominance of the  $3/2^+$  resonance in all reactions initiated by D+T at low energies leads to the expectation that the branching ratio is constant below about 100 keV center-of-mass energy. This means that the ratio of Maxwellian averages of the cross sections at an ion temperature of  $\sim 5$  keV should not deviate significantly from the value seen at low energies in beam-target measurements. Unfortunately, the expected energy dependence is evident only in the more recent beam-target measurements of Cecil *et al.*<sup>4</sup> and of Morgan *et al.*<sup>5</sup> which were measurements of the  $\gamma_0$  branch alone. Since their value for the  $\gamma_0$  transition barely overlaps the upper end of our error bar for the sum of  $\gamma_0 + \gamma_1$  transitions, the results cannot be considered consistent. This gives us cause for further theoretical investigations of the D-T  $\gamma$ -ray spectrum, and of the energy dependence of the branching ratio, at low-energy ICF conditions. The observed difference in the  ${}^3H(d,\gamma){}^3He$  and  ${}^3He(d,\gamma){}^5Li$  branching ratios further motivates investigation of the multichannel  ${}^5He$ - and  ${}^5Li$ -system data simultaneously with a Coulomb-corrected, charge-symmetric R-matrix analysis. To attribute a ratio ( $B_{\gamma/n}^{DT}/B_{\gamma/p}^{D3He}$ ) as low as approximately 0.3 purely to Coulomb corrections poses a theoretical challenge, but is not beyond the realm of possibility.

## VI. CONCLUSION

D-T gamma-to-neutron branching ratio [ ${}^3H(d,\gamma){}^3H(d,n)$ ] under ICF conditions has been determined at OMEGA utilizing the fast temporal response and energy thresholds characteristic of gas Cherenkov  $\gamma$ -ray detectors. Having D-T neutron and  $\gamma$ -ray measurements and the D- ${}^3He$  proton yields

for this purpose allowed a unique determination of this fundamental nuclear property, and an improved understanding of theoretical predictions and previous measurements. In addition to two previously reported methods (absolute and D-<sup>3</sup>He cross-calibration), an *in-situ*  $\gamma$ -ray detector calibration method has been developed and tested at OMEGA using neutron-induced  $\gamma$ -rays. The D-T branching ratio via this puck method was determined by averaging values from four different puck experiments. While further evaluation of 14.1 MeV neutron-induced cross-sections is required to improve accuracy and reduce uncertainty of this puck method, the inferred value corroborates the previously reported value of  $(4.2 \pm 2.0) \times 10^{-5}$   $\gamma/n$ . The influence of ion temperatures in the range of 2–9 keV on the D-T branching ratio was tested using two additional series of implosions, one with a thin glass capsule and the other with cryogenic fuel in a plastic capsule, and found nearly constant D-T branching ratio within error bars. This study illustrates the use of ICF implosions as a new platform in the emerging field of Plasma Nuclear Science<sup>36,37</sup> to augment traditional accelerator-based nuclear physics.

## ACKNOWLEDGMENTS

The authors thank the OMEGA and HI $\gamma$ S operations, engineering, and scientific staff who supported this work. This work was supported by LANL ICF Program, NLUF/DOE (Grant No. DE-FG03-03SF2269), and FSC/DOE (Grant No. DE-FC02-04ER54789).

- <sup>1</sup>Y. Kim, J. M. Mack, H. W. Herrmann, C. S. Young, G. Hale, S. Caldwell, N. Hoffman, S. C. Evans, T. J. Sedillo, A. McEvoy, J. Langenbrunner, H. H. Hus, M. A. Huff, S. Batha, C. J. Horsfield, M. S. Rubery, W. J. Garbett, W. Stoeffl, E. Grafil, L. Bernstein, J. A. Church, D. B. Sayre, M. J. Rosenberg, C. Waugh, H. G. Rinderknecht, M. Gatun Johnson, A. B. Zylstra, J. A. Frenje, D. T. Casey, R. D. Petrasso, E. Kirk Miller, V. Yu. Glebov, C. Stoeckl, and T. C. Sangster, "Determination of D-T branching ratio at inertial confinement fusion conditions" *Phys. Rev. C* (submitted).
- <sup>2</sup>F. Ajzenberg Selove, *Nucl. Phys. A*, **490**, 1 (1988).
- <sup>3</sup>J. M. Mack, R. R. Berggren, S. E. Caldwell, C. R. Christensen, S. C. Evans, J. R. Faulkner Jr., R. L. Griffith, G. M. Hale, R. S. King, D. K. Lash, R. A. Lerche, J. A. Oertel, D. M. Pacheco, and C. S. Young, *Radiat. Phys. Chem.* **75**, 551 (2006).
- <sup>4</sup>F. E. Cecil and F. J. Wilkinson III, *Phys. Rev. Lett.* **53**(8), 767 (1984).
- <sup>5</sup>G. L. Morgan, P. W. Lisowski, S. A. Wender, R. E. Brown, N. Jarmie, J. F. Wilkerson, and D. M. Drake, *Phys. Rev. C* **33**(4), 1224 (1986).
- <sup>6</sup>J. E. Kammeraad, J. Hall, K. E. Sale, C. A. Barnes, S. E. Kellogg, and T. R. Wang, *Phys. Rev. C* **47**(1), 29 (1993).
- <sup>7</sup>W. Buss, H. Waffler, and B. Ziegler, *Phys. Lett.* **4**(3), 198 (1963).
- <sup>8</sup>A. Kosiara and H. B. Willard, *Phys. Lett.* **32B**(2), 99 (1970).
- <sup>9</sup>V. M. Bezotosnyi, V. A. Zhmailo, L. M. Surov, and M. S. Shvetsov, *Sov. J. Nucl. Phys.* **10**(3), 127 (1970).
- <sup>10</sup>M. J. Balbes, J. C. Riley, G. Feldman, H. R. Weller, and D. R. Tilley, *Phys. Rev. C* **49**, 912 (1994).
- <sup>11</sup>C. E. Parker, M.S. thesis, Ohio University, 2011.
- <sup>12</sup>S. Pfalzner, *An Introduction to Inertial Confinement Fusion* (CRC, 2006), p. 13.
- <sup>13</sup>J. Benveniste, A. C. Mitchell, C. D. Schrader, and J. H. Zenger, *Nucl. Phys.* **19**, 448 (1960).
- <sup>14</sup>G. Mitev, P. Colby, N. R. Roberson, H. R. Weller, and D. R. Tilley, *Phys. Rev. C* **34**, 389 (1986).
- <sup>15</sup>R. A. August, H. R. Weller, and D. R. Tilley, *Phys. Rev. C* **35**, 393 (1987).
- <sup>16</sup>R. R. Berggren, S. E. Caldwell, J. R. Faulkner, Jr., R. A. Lerche, J. M. Mack, K. J. Moy, J. A. Oertel, and C. S. Young, *Rev. Sci. Instrum.* **72**(1), 873 (2001).
- <sup>17</sup>J. M. Mack, S. E. Caldwell, S. C. Evans, T. J. Sedillo, D. C. Wilson, C. S. Young, C. J. Horsfield, R. L. Griffith, and R. A. Lerche, *Rev. Sci. Instrum.* **77**, 10E728 (2006).
- <sup>18</sup>H. W. Herrmann, J. M. Mack, C. S. Young, R. M. Malone, W. Stoeffl, and C. J. Horsfield, *Rev. Sci. Instrum.* **79**, 10E531 (2008).
- <sup>19</sup>H. W. Herrmann, C. S. Young, J. M. Mack, Y. H. Kim, A. McEvoy, S. Evans, T. Sedillo, S. Batha, M. Schmitt, D. C. Wilson, J. R. Langenbrunner, R. Malone, M. I. Kaufman, B. C. Cox, B. Frogget, E. K. Miller, Z. A. Ali, T. W. Tunnell, W. Stoeffl, C. J. Horsfield, and M. Rubery, *J. Phys.: Conf. Ser.* **244**, 032047 (2010).
- <sup>20</sup>H. W. Herrmann, N. Hoffman, D. C. Wilson, W. Stoeffl, L. Dauffy, Y. H. Kim, A. McEvoy, C. S. Young, C. S. Mack, C. J. Horsfield, M. Rubery, E. K. Miller, and Z. A. Ali, *Rev. Sci. Instrum.* **81**, 10D333 (2010).
- <sup>21</sup>V. Yu. Glebov, C. Stoeckl, T. C. Sangster, S. Roberts, G. J. Schmid, R. A. Lerche, and M. J. Moran, *Rev. Sci. Instrum.* **75**, 3559 (2004).
- <sup>22</sup>A. Csoto and G. M. Hale, *Phys. Rev. C* **55**, 536 (1997).
- <sup>23</sup>C. J. Horsfield, M. S. Rubery, H. W. Herrmann, Y. H. Kim, J. M. Mack, C. S. Young, S. E. Caldwell, S. C. Evans, T. S. Sedillo, A. M. McEvoy, N. Hoffman, M. A. Huff, J. Langenbrunner, G. Hale, D. C. Wilson, W. Stoeffl, E. M. Grafil, E. K. Miller, and V. Glebov, *Bull. Am. Phys. Soc.* **56**, 193 (2011).
- <sup>24</sup>J. A. Halbleib, R. P. Kensek, G. D. Valdez, S. M. Seltzer, and M. J. Berger, *IEEE Trans. Nucl. Sci.* **39**(4), 1025 (1992).
- <sup>25</sup>J. V. Jelly, *Cherenkov Radiation and Its Applications* (Pergamon, London, 1958), p. 22.
- <sup>26</sup>M. S. Rubery, C. J. Horsfield, H. W. Herrmann, Y. Kim, J. M. Mack, C. S. Young, S. E. Caldwell, S. C. Evans, T. J. Sedillo, A. McEvoy, E. K. Miller, W. Stoeffl, Z. Ali, and J. Toebbe, *Rev. Sci. Instrum.* **81**, 10D328 (2010).
- <sup>27</sup>D. G. Hicks, C. K. Li, F. H. Seguin, A. K. Ram, J. A. Frenje, R. D. Petrasso, J. M. Soares, V. Yu. Glebov, D. D. Meyerhofer, S. Roberts, C. Sorce, C. Stoeckl, T. C. Sangster, and T. W. Phillips, *Phys. Plasmas* **7**(12), 5106 (2000).
- <sup>28</sup>F. H. Seguin, J. A. Frenje, C. K. Li, D. G. Hicks, S. Kurebayashi, J. R. Rygg, B.-E. Schwartz, R. D. Petrasso, S. Roberts, J. M. Soares, D. D. Meyerhofer, T. C. Sangster, J. P. Knauer, C. Sorce, V. Yu. Glebov, C. Stoeckl, T. W. Phillips, R. J. Leeper, K. Fletcher, and S. Padalino, *Rev. Sci. Instrum.* **74**(2), 975 (2003).
- <sup>29</sup>F. E. Cecil, D. M. Cole, R. Philbin, N. Jarmie, and R. Brown, *Phys. Rev. C* **32**(3), 690 (1985).
- <sup>30</sup>Y. Kim, H. W. Herrmann, S. Evans, T. Sedillo, J. R. Langenbrunner, C. S. Young, J. M. Mack, A. McEvoy, C. J. Horsfield, M. Rubery, Z. Ali, and W. Stoeffl, *J. Phys.: Conf. Ser.* **244**, 032050 (2010).
- <sup>31</sup>N. M. Hoffman, H. W. Herrmann, Y. H. Kim, H. H. Hsu, C. J. Horsfield, M. S. Rubery, D. C. Wilson, W. Stoeffl, C. S. Young, J. M. Mack, E. K. Miller, E. Grafil, S. C. Evans, T. J. Sedillo, V. Yu. Glebov, and T. Duffy, "In situ calibration of the Gamma Reaction History instrument using reference samples ("puck") for areal density measurements," *J. Phys.: Conf. Ser.* (submitted).
- <sup>32</sup>M. B. Chadwick, P. Oblozinský, M. Herman, N. M. Greene, R. D. McKnight, D. L. Smith, P. G. Young, R. E. MacFarlane, G. M. Hale, S. C. Frankle, A. C. Kahler, T. Kawano, R. C. Little, D. G. Madland, P. Moller, R. D. Mosteller, P. R. Page, P. Talou, H. Trellue, M. C. White, W. B. Wilson, R. Arcilla, C. L. Dunford, S. F. Mughabghab, B. Pritychenko, D. Rochman, A. A. Sonzogni, C. R. Lubitz, T. H. Trumbull, J. P. Weinman, D. A. Brown, D. E. Cullen, D. P. Heinrichs, D. P. McNabb, H. Derrien, M. E. Dunn, N. M. Larson, L. C. Leal, A. D. Carlson, R. C. Block, J. B. Briggs, E. T. Cheng, H. C. Huria, M. L. Zerkle, K. S. Kozier, A. Courcelle, V. Pronyaev and S. C. van der Marck, *Nuclear Data Sheets* **107**(12), 2931 (2006).
- <sup>33</sup>X-5 Monte Carlo Team, MCNP-A General Monte Carlo N-Particle transport Code, Version 5 (2003).
- <sup>34</sup>S. Atzeni and J. Meyer-ter-Vehn, *The Physics of Inertial Fusion: Beam Plasma Interaction, Hydrodynamics, Hot Dense Matter* (Oxford University Press, Oxford, 2009), p. 16.
- <sup>35</sup>D. T. Casey, Ph.D. dissertation, Massachusetts Institute of Technology, 2012.
- <sup>36</sup>J. A. Frenje, C. K. Li, F. H. Seguin, D. T. Casey, R. D. Petrasso, D. P. McNabb, P. Navratil, S. Quaglioni, T. C. Sangster, V. Yu. Glebov, and D. D. Meyerhofer, *Rhys. Rev. Lett.* **107**, 122502 (2011).
- <sup>37</sup>D. T. Casey, J. A. Frenje, M. Gatun Johnson, M. J.-E. Manuel, H. G. Rinderknecht, N. Sinenian, F. H. Seguin, C. K. Li, R. D. Petrasso, P. B. Radha, J. A. Delettrez, V. Yu. Glebov, D. D. Meyerhofer, T. C. Sangster, D. P. McNabb, P. A. Amendt, R. N. Boyd, J. R. Rygg, H. W. Herrmann, Y. H. Kim, and A. D. Bacher, "Evidence for stratification of deuterium-tritium fuel in inertial confinement fusion implosions," *Phys. Rev. Lett.* **108**, 075002 (2012).